Projections of Tropical Heat Stress Constrained by Atmospheric Dynamics

Yi Zhang[1], Isaac Held[1], and Stephan Fueglistaler[1]

[1]Princeton University

October 30, 2023

Abstract

Extreme heat under global warming is a concerning issue for the growing tropical population. However, model projections of extreme temperatures, a widely used metric for extreme heat, are uncertain on regional scales. In addition, humidity also needs to be taken into account in order to estimate the health impact of extreme heat. Here we show that an integrated temperature-humidity metric for the health impact of heat, namely the extreme wet-bulb temperature (TW), is controlled by established atmospheric dynamics and thus can be robustly projected on regional scales. For each 1°C of tropical mean warming, global climate models project extreme TW (the annual maximum of daily-mean or 3-hourly values) to increase roughly uniformly between 20°S and 20°N latitude by about 1°C. This projection is consistent with the theoretical expectation based on tropical atmospheric dynamics, and observations over the past 40 years, which gives confidence to the model projection. For a 1.5°C warmer world, the likely (66 per cent confidence interval) increase of regional extreme TW is projected to be 1.33-1.49°C, whereas the uncertainty of projected extreme temperatures is 3.7 times as large. These results suggest that limiting global warming to 1.5°C will prevent most of the tropics from reaching a TW of 35°C, the limit of human adaptation.

Projections of Tropical Heat Stress Constrained by Atmospheric Dynamics

Yi Zhang[*,1], Isaac Held[1], Stephan Fueglistaler[1,2]

[1]Program in Atmospheric and Oceanic Sciences, Princeton University, Sayre Hall, Princeton, NJ 08540, USA.

[2]Department of Geosciences, Princeton University, Guyot Hall, Princeton, NJ 08544, USA.

[*]Correspondence to: yz8@princeton.edu

Abstract

Extreme heat under global warming is a concerning issue for the growing tropical population. However, model projections of extreme temperatures, a widely used metric for extreme heat, are uncertain on regional scales. In addition, humidity also needs to be taken into account in order to estimate the health impact of extreme heat. Here we show that an integrated temperature-humidity metric for the health impact of heat, namely the extreme wet-bulb temperature (TW), is controlled by established atmospheric dynamics and thus can be robustly projected on regional scales. For each 1°C of tropical mean warming, global climate models project extreme TW (the annual maximum of daily-mean or 3-hourly values) to increase roughly uniformly between 20°S and 20°N latitude by about 1°C. This projection is consistent with theoretical expectation based on tropical atmospheric dynamics, and observations over the past 40 years, which gives confidence to the model projection. For a 1.5°C warmer world, the likely (66 per cent confidence interval) increase of regional extreme TW is projected to be 1.33-1.49°C, whereas the uncertainty of projected extreme temperatures is 3.7 times as large. These results suggest that limiting global warming to 1.5°C will prevent most of the tropics from reaching a TW of 35°C, the limit of human adaptation.

Main

The impact of global warming on local extreme heat is projected to be detectable earliest in

the tropics[1–3] where baseline temperatures are already high. In addition, countries located

between 20°S and 20°N latitude will soon become major contributors to the global population

growth,[4] and there is thus a pressing need for accurate projections of extreme heat in the

tropics down to regional scales.

The most widely used metric for extreme heat has been the extreme temperature. However, projections of extreme temperatures have large regional uncertainty arising from insufficient model representation of important land processes.[5] Moreover, to facilitate the estimation of heat-induced health impact (or heat stress), the effect of humidity should also be included,[6,7] and this is because the major way for humans to lose metabolic heat in hot weather is evaporative cooling (sweating),[8,9] the efficiency of which anti-correlates with humidity. In particular, the inclusion of humidity is necessary for assessing heat stress in the tropics, the warmest and the most humid places on the Earth.

The importance of humid heat has been increasingly recognized.[10,11] Studies have shown that increased humidity with temperature following the Clausius-Clapeyron relationship can worsen summer heat stress in the tropics,[12,13] while other work has noticed a reduction in either relative humidity[14] or specific humidity[15] on the hottest days (not limited to the tropics). Given the possibility that humidity can interact with temperature in extreme heat, it is necessary to better quantify and improve our mechanistic understanding for the control of humid heat.

Here, we use the extreme wet-bulb temperature (TW), an integrated temperature-humidity

metric for heat stress (see Methods). TW by definition is the lowest temperature that human skin can be cooled to through evaporation of sweat. Therefore, the closer TW is to the upper limit of human skin temperature (around 35°C), the more intolerable the heat is, with a survival limit of TW=35°C[16] (Note that high TW values below this survival limit also have adverse health impact). Furthermore, TW is a major component in the wet-bulb globe temperature (WBGT; See Methods)[17] which is the standard metric for workplace heat stress. In this paper, we argue that the regional extreme TW in the tropics is mainly controlled by robust atmospheric dynamics that have been established previously,[18–21] rather than local processes that are of more uncertainty. Therefore, tropical extreme TW can be robustly projected on regional scales under global warming.

Global climate model projections

Fig. 1a shows the projections of extreme TW (TW_{max}) and extreme temperatures (T_{max}) by 22 global climate models (Table S1) from the Coupled Model Intercomparison Project phase 5 (CMIP5)[22] under the Representative Concentration Pathway 8.5 (RCP 8.5) emission scenario (Note that TW_{max} and T_{max} mostly refer to the annual maximum of *daily* mean values in this paper, and refer to the annual maximum of *3-hourly* values when specifically stated). The multi-model mean of T_{max} averaged over tropical land within 20°S-20°N warms faster than the tropical mean temperature. However, TW_{max} closely follows the tropical mean warming, similar to an earlier finding using an atmospheric model coupled to a slab ocean.[16] These results also hold when analysing 3-hourly data that resolve the diurnal cycle from two models (GFDL-CM3 and IPSL-CM5A-LR) (Fig. 1b,c).
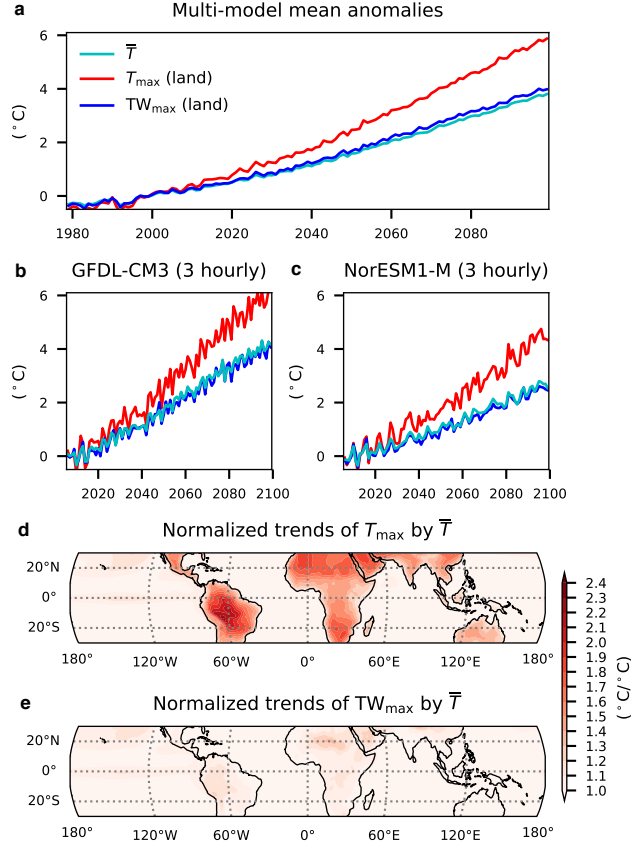
4

Figure 1: TW$_{max}$ **and** T_{max} **trends in climate models under RCP 8.5. a**, Multi-model-mean time series of the tropical-mean (20°S-20°N) temperature ($\overline{T}$; cyan), land-mean T_{max} (red), and land-mean TW$_{max}$ (blue). **b** and **c**, The same as **a** but using the annual-maximum 3-hourly values for T_{max} and TW$_{max}$ for two individual models. **d** and **e**, Multi-model-mean location-specific T_{max} and TW$_{max}$ trends normalized by $\overline{T}$ trends.

67 Figs. 1d,e show T_{max} and TW$_{max}$ trends for all locations normalized by the tropical mean

68 warming under RCP 8.5. T_{max} warming is spatially inhomogeneous over land ranging from

69 1.0°C to 2.3°C for each 1°C of tropical mean warming (Fig. 1d) consistent with previous

5

findings. In contrast, we find that increases of TW_{max} has no significant land-ocean contrast ranging from 0.8°C to 1.3°C for each 1°C of tropical mean warming (Fig. 1e). Using the annual-maximum 3-hourly TW for TW_{max} does not change this result (Fig. S1).
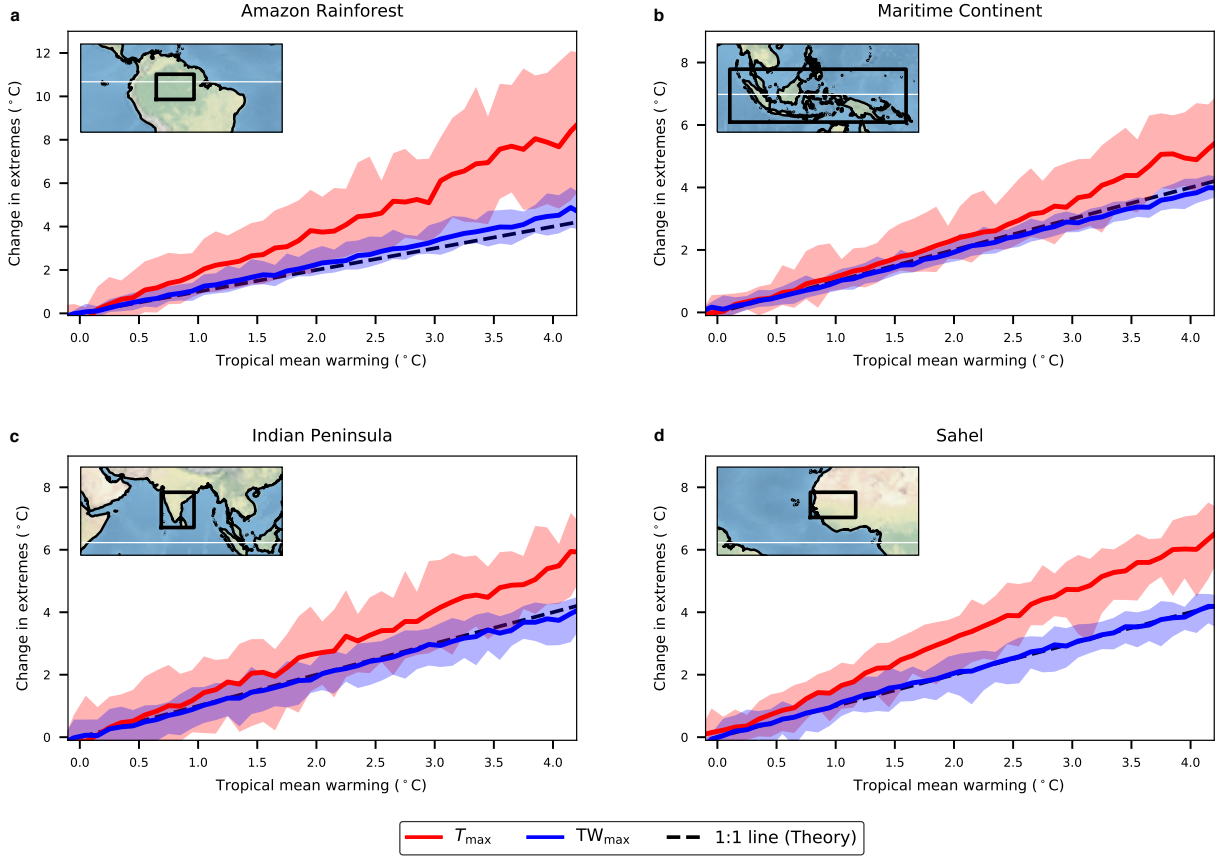

Figure 2: **Model agreement on regional** TW_{max} **projections.** Multi-model means (lines) and spreads (2.5-97.5th percentiles; shading) for regional T_{max} (red) and TW_{max} (blue) as a function of the tropical mean warming are shown for four regions, namely **a** Amazon rainforest, **b** Maritime Continent, **c** Indian Peninsula, and **d** Sahel (Only land data within the black frames on the maps are sampled). The dashed black lines indicate the 1:1 ratio.

The spatially uniform TW_{max} trend (Fig. 1e) is not a cancellation of errors among different models. Instead, all models show good agreement on TW_{max} trend, even down to

regional scales. Fig. 2 shows the model spread (2.5-97.5th percentiles) of $T_{\max}$ and $TW_{\max}$ projections for four selected regions that have caught substantial attention in the literature, namely the Amazon rainforest, the Maritime Continent, the Indian peninsula, and the Sahel. Projected $T_{\max}$ warming has large spread among models, which is especially prominent in the Amazon rainforest, consistent with earlier analysis.[5] However, for regional $TW_{\max}$, all 22 climate models project a close to 1:1 ratio with the tropical mean warming. Using the annual maximum of 3-hourly TW does not change this result (Fig. S2). Intriguingly, the model spread of $T_{\max}$ tends to grow with the amplitude of the projected warming (pronounced for the Amazon rainforest and the Maritime Continent), whereas the model spread of $TW_{\max}$ does not show evident growth within the range of simulated warming (roughly 4°C). That the inter-model spread is much less for $TW_{\max}$ projections than for $T_{\max}$ is also true for other tropical land regions (Fig. S3).

To summarize, global climate models predict that $TW_{\max}$ will increase roughly uniformly in the tropics by about 1°C for each 1°C of tropical mean warming. Models show wide spread on regional $T_{\max}$ projections but agree very well upon regional $TW_{\max}$.

Theoretical support

For a theoretical projection of $TW_{\max}$, we argue that tropical atmospheric dynamics exert a strong, tropics-wide control on local $TW_{\max}$. This control is through the functional relationship between TW and moist static energy (MSE; Fig. S4) which is a variable regulated by atmospheric dynamics. In the tropics, the free-tropospheric temperature is roughly uniform in the horizontal as a result of the weak effect of the Earth's rotation. This horizontally

7

uniform temperature, which is determined by the near-surface MSE in regions of deep convection, sets the upper bound for MSE at all locations. Indeed, the maximum near-surface MSE is roughly uniform within 20°S-20°N (even more uniform than the time-mean MSE; Fig.S5a,b), and the spatial pattern of TW_{max} closely follows the uniformity of the maximum MSE (Fig. S5c). As this upper bound for near-surface MSE and, equivalently, for TW is a common one over land or over ocean,[21] we expect that changes in TW_{max} should also be roughly equal over land and over ocean under global warming:

$$\Delta TW_{max,Land} \approx \Delta TW_{max,Ocean} \tag{1}$$

Eq. (1) thus provides a handle on TW_{max} over land which is challenging to predict due to various land types and land processes, as a theoretical projection for TW_{max} over ocean can be made relatively easily. Near the ocean surface, air is close to saturation and TW changes are approximately equal to temperature changes (exactly equal when air is saturated), and $\Delta TW_{max,Ocean}$ is thus approximately equal to the change in the warmest SSTs. Therefore, 1°C of $\Delta TW_{max,Land}$ is accompanied by 1°C of warming of the warmest SSTs according to Eq. (1). Furthermore, the area dominance of the ocean and the relatively constant shape of SST histogram under global warming (Fig. S6) together result in a 1:1 correspondence between warming of the warmest SSTs and the tropical mean temperature (While there is potential for differences between changes in these relatively warm SSTs and the tropical mean SST,[23–25] we find these differences to be small enough that they do not undermine the theoretical considerations here). We thus expect $\Delta TW_{max,Land}$ roughly equals the tropical mean warming.

Global climate models shown in Figs. 1, 2 are consistent with the above theoretical

8

considerations. For each 1°C of tropical mean warming, models on average give 1.05 °C of $\Delta TW_{max,Land}$, 0.93°C of $\Delta TW_{max,Ocean}$, and 0.91°C of the warmest-quartile-mean SST increase, all close to 1°C.

The non-local control of TW_{max} by the warmest SSTs seems to be at odds with the perception that these extreme events are driven by rare local meteorology, and this controversy deserves some clarification. While TW_{max} events are driven by local processes, the potential magnitude of TW_{max} is largely set by the uniform free tropospheric temperature. The effectiveness of this non-local control is evident in the uniformity of TW_{max} increases in Fig. 1d and the good agreement across models in Fig. 2, neither of which can be explained by the heterogeneity of local processes. Moreover, the existence of such a non-local control within the tropics also explains why the tropics are consistently warm and humid, but the highest TW and WBGT are observed in the subtropics.[13, 26, 27] These considerations thus support the picture that the magnitude of ΔTW_{max} across tropical land regions is set by the warmest SSTs and not local processes or the spatial pattern of SST.

Observational evidence

From 1979 to 2018, the tropical (20°S-20°N) land mean T_{max} trend has a 95% confidence interval of 0.24-0.31°C/decade, which is almost three times of the tropical mean warming of 0.08-0.12°C/decade based on ERA-Interim reanalysis[28] (Fig. 3a). TW_{max} has a trend of 0.05-0.10°C/decade, very similar to the tropical mean warming, and the interannual variabilities of the two are highly correlated with a correlation coefficient of 0.85 (Fig. 3a). Using the annual-maximum 3-hourly TW from ERA-Interim yields very similar anomalies, though the
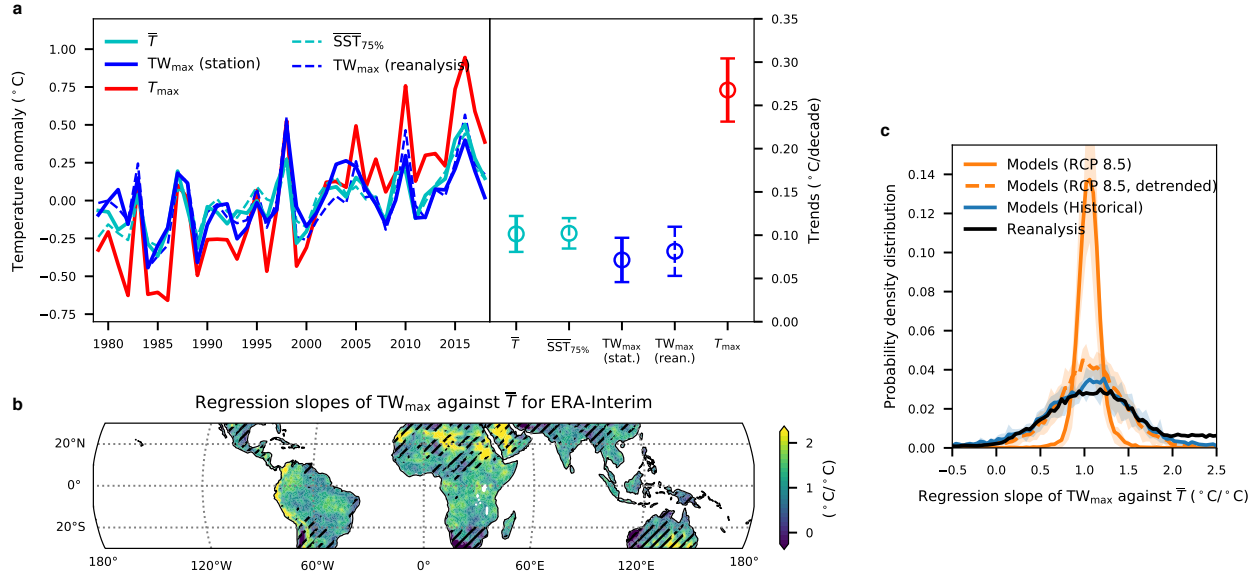
Figure 3: TW_{max} **in observations and reanalysis data. a**, Time series and corresponding linear trends of tropical mean temperature ($\overline{T}$; solid cyan), land-mean T_{max} (red), land-mean TW_{max} from stations (solid blue) and ERA-Interim (dashed blue), and the warmest-quartile-mean SST from HadISST (dashed cyan) for 1979-2018 (20°S-20°N). The confidence intervals for the linear trends represent 95% significance assuming that the detrended annual data points are independent. **b**, Linear regression slopes of local TW_{max} onto $\overline{T}$ in the interannual variabilities (linear trends removed) from ERA-Interim for 1979-2018. Regions where TW_{max} and $\overline{T}$ are not correlated on a 95% significance level are hatched. **c**. Histograms of regression slopes of local TW_{max} onto $\overline{T}$ (linear trends removed) for 1979-2005 in ERA-Interim (black solid) and models (blue solid), and for the global warming simulations in models (orange dashed). The same histogram for non-detrended global warming simulations (Fig. 1e) is also shown (orange solid). Shading indicates the 25-75th percentiles of models.

10

longterm trend is smaller (Fig. S7). Furthermore, station measurements of TW provided by HadISD[29] (see Methods; Fig. S8) show that TW_{max} averaged over tropical stations is highly correlated with that from ERA-Interim and has a similar trend of 0.05-0.10°C/decade (Fig. 3a). The consistency of reanalysis data with station observations and the theory lends support to the quality of the reanalysis data over tropical land.

The warmest-quartile-mean SST (the average of the top 25% of monthly SST at all grid points within each year) from HadISST[30] is highly correlated with land-mean TW_{max} and has a similar trend of 0.08-0.12°C/decade (Fig. 3a). Satellite SST observations and station TW observations are largely independent, and the very good consistency in their extreme values lends strong support to the aforementioned argument that TW_{max} over land is coupled to the warmest SSTs. Strong El Niño events have the potential of warming the warmest SSTs and, as a result, affect TW_{max} over land (e.g., 1998 in Fig. 3a).

Location-specific evaluation of long-term TW_{max} trends for the observations suffers from the smallness of the warming signal, but interannual variability of SST provides room for testing the 1:1 relationship with TW_{max}. Regression slopes of TW_{max} (ERA-Interim) onto the tropical mean temperature (linear trends removed) is relatively uniform over most of the land regions within 20°S-20°N (Fig. 3b) with a mode value close to 1 (Fig. 3c). This relationship loosens in the subtropics (indicated by the hatching in Fig. 3b), consistent with the latitudinal range where the theory works.[21] That the Andes and the southern edge of the Sahara have much higher TW_{max} sensitivity does not violate the proposed theory, as climatological TW_{max} in those regions is too low to trigger convection and thus not constrained by the aforementioned mechanism. The standard deviation of these slopes in the reanalysis is larger than that for the global warming simulations shown in Fig. 1e (Fig.

3c). A likely explanation is that the spatial pattern of TW_{max} can change in the interannual variability and such a spatial rearrangement can cause a spread in the regression slopes but does not affect the tropical averages shown in Fig. 3a. Indeed, global climate models also show a similar spread of TW_{max} trends under historical radiative forcing, and the removal of longterm trends in the global warming simulations for the same set of models also result in a similar spread (Fig. 3c). Therefore, regional TW_{max} trends diagnosed from reanalysis data over the past 40 years are consistent with global climate models. Also for similar reasons, we do not expect every station to give the same TW_{max} trend either.

While we do not attempt to formulate an attribution statement for the TW_{max} trend over land seen in Fig. 3a, we note that the tight relationship in the overall trend as well as higher frequency variability strongly suggests that any attribution statements for the tropical mean temperature or SST can also be applied to TW_{max}.

Implications for the future climate

Consistency of model results with the theory and observations lends strong support to the capability of global climate models in properly simulating regional TW_{max} increases. In a 1.5°C warmer world, the projected 66 per cent confidence interval (equivalent to IPCC's "likely range") for TW_{max} increases across all tropical land regions (20°S-20°N) is 1.33-1.49°C, consistent with the simulated tropical mean warming of ~1.4°C in a 1.5°C warmer climate (Fig. 4). On the other hand, projected T_{max} increases have a wider distribution, the absolute (relative) standard deviation of which is 3.7 (1.8) times of that of TW_{max} increases. The reduction in uncertainty is more pronounced for regions where T_{max} projections are most
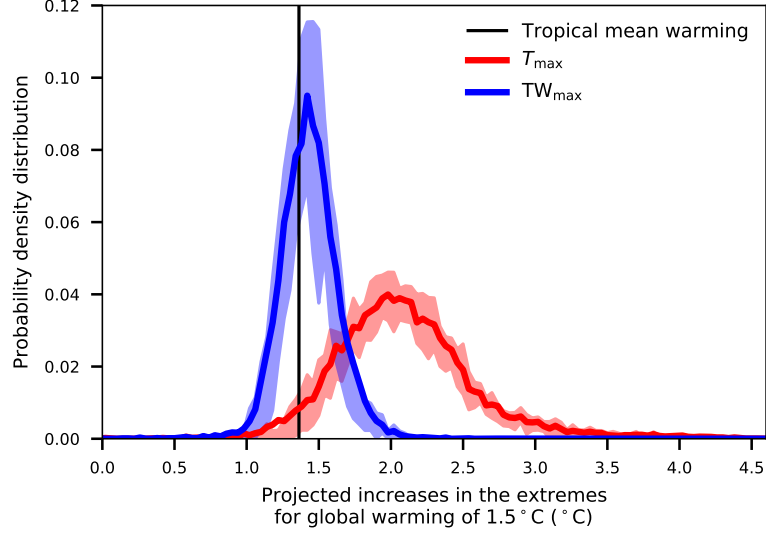
Figure 4: **Uncertainty of $T_{\max}$ and $TW_{\max}$ projection in a 1.5°C warmer world (land between 20°S-20°N).** Distributions of model projected $TW_{\max}$ increases (blue) and $T_{\max}$ increases (red) under RCP 8.5 at 1.5°C of global mean warming are shown. The distributions are constructed by linearly regressing local $T_{\max}$ and $TW_{\max}$ increases onto global mean warming and taking the regression values at 1.5°C of global mean warming. Solid lines show the average distribution of all models and the shading indicates the 25-75th percentiles across models.

182   uncertain. For example, in the Amazon rainforest and the Maritime Continent (Fig. 2), the

183   absolute (relative) uncertainty of $T_{\max}$ increases is around 4 (2.5) times of that of $TW_{\max}$

184   increases.

185   Our results imply that curtailing global mean warming will have a proportional effect on

186   regional $TW_{\max}$ in the tropics. The maximum 3-hourly TW (ERA-Interim) ever experienced

187   in the past 40 years by 99.98% of the land area within 20°S-20°N is below 33 °C. Therefore, a

188   1.5°C or 2°C warmer world will likely exempt the majority of the tropical area from reaching

the survival limit of 35°C. However, there exists little knowledge on safety thresholds for TW besides the survival limit,[11] and 1°C of TW increase could have adverse health impact equivalent to that of several degrees of temperature increase. TW will thus have to be better calibrated to health impact before wider societal implementation. Nonetheless, the confidence in TW_{max} projection provided in this work still raises the confidence in projections of other calibrated heat stress metrics that accounts for TW, such as the WBGT.

References

[1] Mahlstein, I., Knutti, S., Solomon, S. & Portmann, R. W. Early onset of significant local warming in low latitude countries. *Environ. Res. Lett.* **6**, 034009 (2011).

[2] Coumou, D., Robinson, A. & Rahmstorf, S. Global increase in record-breaking monthly-mean temperatures. *Clim. Change* **118**, 771-782 (2013).

[3] Hoegh-Guldberg, O. *et al. Global Warming of 1.5° C. An IPCC Special Report on the impacts of global warming of 1.5° C above pre-industrial levels and related global greenhouse gas emission pathways, in the context of strengthening the global response to the threat of climate change, sustainable development, and efforts to eradicate poverty* (eds Masson-Delmotte, V. *et al.*) Ch. 3 (In Press).

[4] United Nations, Department of Economic and Social Affairs, Population Division (2019). *World population prospects 2019: Highlights* (ST/ESA/SER.A/423).

[5] Vogel, M. *et al.* Regional amplification of projected changes in extreme temperatures strongly controlled by soil moisture-temperature feedbacks. *Geophys. Res. Lett.* **44**, 1511-1519 (2017).

[6] Kovats, R. S. & Hajat, S. Heat stress and public health: a critical review. *Annu. Rev. Public Health* **29**, 41-55 (2008).

[7] Mitchell, D. *et al.* Attributing human mortality during extreme heat waves to anthropogenic climate change. *Environ. Res. Lett.* **11**, 074006 (2016).

[8] Hardy, J. D., Du Bois, E. F. & Soderstrom, G. F. Basal metabolism, radiation, convection and vaporization at temperatures of 22 to 35°C. *J. Nutr.* **15**, 477-497 (1938).

[9] Hardy, J. D. & Stolwijk, J. A. Partitional calorimetric studies of man during exposures to thermal transients. *J. Appl. Physiol.* **21**, 1799-1806 (1966).

[10] Mora, C. *et al.* Global risk of deadly heat. *Nat. Clim. Change* **7**, 501-505 (2017).

[11] Sherwood, S. C. How important is humidity in heat stress? *J. Geophys. Res. Atmos.* **123**, 808-810 (2018).

[12] Delworth, T. L., Mahlman, J. D. & Knutson, T. R. Changes in heat index associated with CO2-induced global warming. *Clim. Change* **43**, 369-386 (1999).

[13] Willett, K. M. & Sherwood, S. Exceedance of heat index thresholds for 15 regions under a warming climate using the wet-bulb globe temperature. *Int. J. Climatol.* **32**, 161-177 (2012).

[226] [14] Fischer, E. M. & Knutti, R. Robust projections of combined humidity and temperature extremes. *Nat. Clim. Change* **3**, 126-130 (2013).

[228] [15] Coffel, E.D., Horton, R. M., Winter, J. M. & Mankin, J. S. Nonlinear increases in extreme temperatures paradoxically dampen increases in extreme humid-heat. *Environ. Res. Lett.* **14**, 084003 (2019).

[231] [16] Sherwood, S. C & Huber, M. An adaptability limit to climate change due to heat stress. *Proc. Natl. Acad. Sci.* **107**, 9552-9555 (2010).

[233] [17] International Organization for Standardization. (2017). Ergonomics of the thermal environment — Assessment of heat stress using the WBGT (wet bulb globe temperature) index (ISO Standard No. 7243:2017). https://www.iso.org/standard/67188.html

[236] [18] Byrne, M. P. & O'Gorman, P. A. Land-ocean warming contrast over a wide range of climates: Convective quasi-equilibrium theory and idealized simulations. *J. Clim.* **26**, 4000–4016 (2013).

[239] [19] Byrne, M. P. & O'Gorman, P. A. Link between land-ocean warming contrast and surface relative humidities in simulations with coupled climate models. *Geophys. Res. Lett.* **40**, 5223-5227 (2013).

[242] [20] Byrne, M. P. & O'Gorman, P. A. Trends in continental temperature and humidity directly linked to ocean warming. *Proc. Natl. Acad. Sci.* **115**, 4863-4868 (2018).

[244] [21] Zhang, Y. & Fueglistaler, S. How tropical convection couples high moist static energy over land and ocean. *Geophys. Res. Lett.* **47**, e2019GL086387 (2020).

[246] [22] Taylor, K. E., Stouffer, R. J. & Meehl, G. A. An overview of CMIP5 and the experiment

[247] design. *Bull. Am. Meteorol. Soc.* **93** 485-498 (2012).

[248] [23] Sobel, A. H., Held, I. M. & Bretherton, C. S. The ENSO Signal in Tropical Tropospheric

[249] Temperature *J. Clim.* **15**, 2702-2706 (2002).

[250] [24] Flannaghan, T. J. *et al.* Tropical temperature trends in Atmospheric General Circulation

[251] Model simulations and the impact of uncertainties in observed SSTs. *J. Geophys. Res.*

[252] **119**, 327-337 (2014).

[253] [25] Fueglistaler, S. Observational evidence for two modes of coupling between sea surface

[254] temperatures, tropospheric temperature profile and shortwave cloud radiative effect in the

[255] tropics. *Geophys. Res. Lett.* **46**, 9890-9898 (2019).

[256] [26] Pal, J. S. & Eltahir, E. A. B. Future temperature in southwest asia projected to exceed a

[257] threshold for human adaptability. *Nat. Clim. Change* **6**, 197–200 (2016).

[258] [27] Im, E., Pal, J. S & Eltahir, E. A. B. Deadly heat waves projected in the densely populated

[259] agricultural regions of South Asia. *Sci. Adv.* **3** e1603322 (2017).

[260] [28] Dee, D. P. *et al.* The ERA-Interim reanalysis: Configuration and performance of the data

[261] assimilation system. *Q. J. R. Meteorol. Soc.* **137**, 553-597 (2011).

[262] [29] Dunn, R. J. H., Willett, K. M., Parker, D. E. & Mitchell, L. Expanding HadISD: quality-

[263] controlled, sub-daily station data from 1931. *Geosci. Instrum. Methods Data Syst.* **5**, 473-

[264] 491 (2016).

[265] [30] Rayner, N. A. *et al.* Global analyses of sea surface temperature, sea ice, and night marine

[266] air temperature since the late nineteenth century. *J. Geophys. Res. Atmos.* **108**, 4407

[267] (2003).

Methods

Wet-bulb temperature (TW). TW is thermodynamically defined as the temperature that an air parcel would have if cooled adiabatically to saturation at constant pressure by evaporation of water into it, all latent heat being supplied by the parcel. This process is enthalpy conserving, therefore $c_p T + Lq = c_p \text{TW} + Lq_{sat}(\text{TW})$, where T and q are the temperature and the specific humidity of an environmental air parcel.[31] TW is empirically defined as the temperature read from the wet-bulb thermometer which is a balance between diffusion of sensible heat from the environment to the saturated surface and the latent heat the other way around. Here we adopt the second definition because it is more relevant for the process of evaporative cooling of sweat. The two definitions give the same result due to the coincidence that the diffusivities of sensible and latent heat are the same. TW is calculated by solving the following equation using Newton's iteration: $c_p T + Lq = c_p \text{TW} + \epsilon L e_{sat}(\text{TW})/p_s$, where T, q, and p_s are temperature, specific humidity, and pressure of the surface-air air, ϵ is the molecular mass ratio of water vapor and air.

Wet-bulb globe temperature (WBGT). WBGT evaluates the heat stress to which a person is exposed used by workers, athletes, and military. It is defined as WBGT $= 0.7\text{TW} + 0.3T_d$ (or WBGT $= 0.7TW + 0.2T_g + 0.1T_d$ to take solar insolation into account), where TW is the wet-bulb temperature, T_g is the globe thermometer temperature, and T_d is the dry-bulb temperature (or actual air temperature).

Station data. Station data from HadISD are selected based on the following procedure: For each station, we first scan though TW measurements for each day and only take the daily averages of those days containing at least 4 measurements. Then, for the years containing

more than 300 daily-mean TW, the annual maximum TW is taken. In the end, stations with at least 20 valid annual-maximum TW values are included in this paper which end up to 293 stations (Fig. S8). For those stations, the average TW is subtracted for each station, then the anomalies are averaged among all stations as is shown in Fig. 3.

Daily-mean and 3-hourly TW from CMIP5 models. CMIP5 models provide surface-air temperature and specific humidity on daily and 3-hourly frequency but not surface pressure. Therefore we interpolate monthly surface pressure piece-wisely to daily frequency for daily TW calculation and ignore the diurnal cycle in surface pressure for 3-hourly TW calculation. The error thus induced in TW is estimated to be less than 0.3°C.

References

[31] Iribarne, J. V. & Godson, W. L. *Atmospheric thermodynamics Ch. 6* (Springer Netherlands, Dordrecht, Netherlands, 1973).

Data Availability

CMIP5 model data provided by the World Climate Research Programme's Working Group on Coupled Modelling and climate modeling groups can be accessed at `https://esgf-node.llnl.gov/projects/cmip5`. ERA-Interim data provided by European Centre for Medium-range Weather Forecast (ECMWF) can be accessed at `https://www.ecmwf.int/en/forecasts/datasets/archive-datasets/reanalysisdatasets/era-interim`. HadISD global sub-daily station dataset (v3.0.1.201909p) provided by Met Office Hadley Centre can be accessed at

Code Availability

The computer code used in this paper is available from Y.Z. (yz8@princeton.edu).

Corresponding Author

Correspondence and requests for materials should be addressed to Y.Z. at yz8@princeton.edu.

Acknowledgements

Author Contributions

Y.Z. conceived the theory, performed the data analysis, and wrote the manuscript. I.H. suggested the examination of observations/reanalysis. S.F. interpreted the widening of TW_{max}

trend distribution in reanalysis (Fig. 3c). All authors discussed the results and edited the

manuscript.

Supplementary Information for "Projections of Tropical Heat Stress Under Global Warming Constrained by Atmospheric Dynamics"

Yi Zhang [1] **Isaac Held** [1] **S. Fueglistaler** [1,2]

[1] Program in Atmospheric and Oceanic Sciences, Princeton University, Sayre Hall, Princeton NJ 08540,

USA.

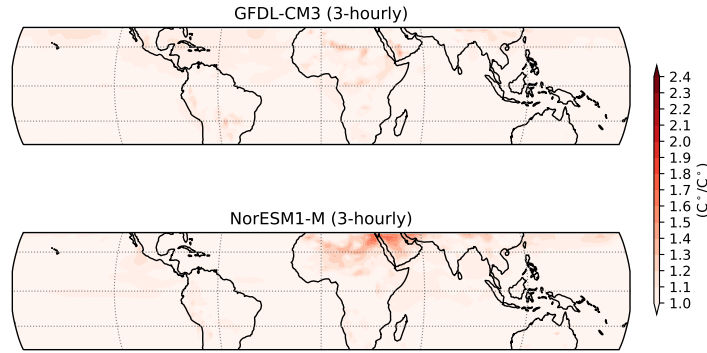[2] Dept. of Geosciences, Princeton University, Guyot Hall, Princeton NJ 08544, USA.

Figure S1. Location-specific $T_{\max}$ (annual-maximum 3-hourly TW) trends normalized by tropical mean warming for GFDL-CM3 and NorESM1-M models.

Figure S2. TW_{max} (annual-maximum 3-hourly TW) increases vs. the tropical mean warming for the four regions in Fig. 2 for GFDL-CM3 and NorESM1-M models.
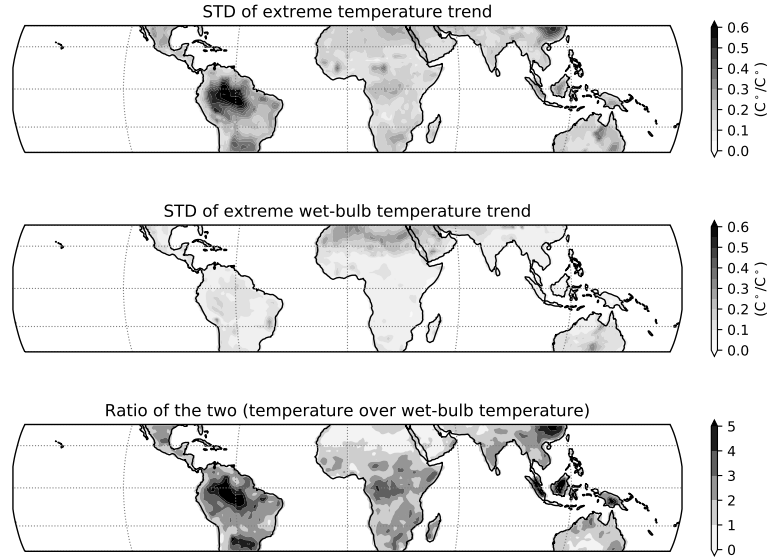

Figure S3. Standard deviations across models of projected normalized trends of T_{max} (upper) and TW_{max} (middle) and the ratios of the two (lower).
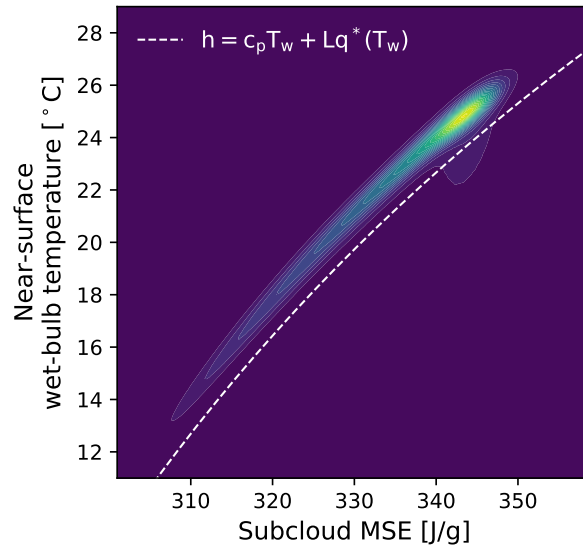
Figure S4. The histogram of 2-m wet-bulb temperature vs. subcloud MSE from ERA-Interim daily data averaged for 2001-2014. The dashed white line shows the theoretical relationship between MSE at sea level and the wet-bulb temperature.
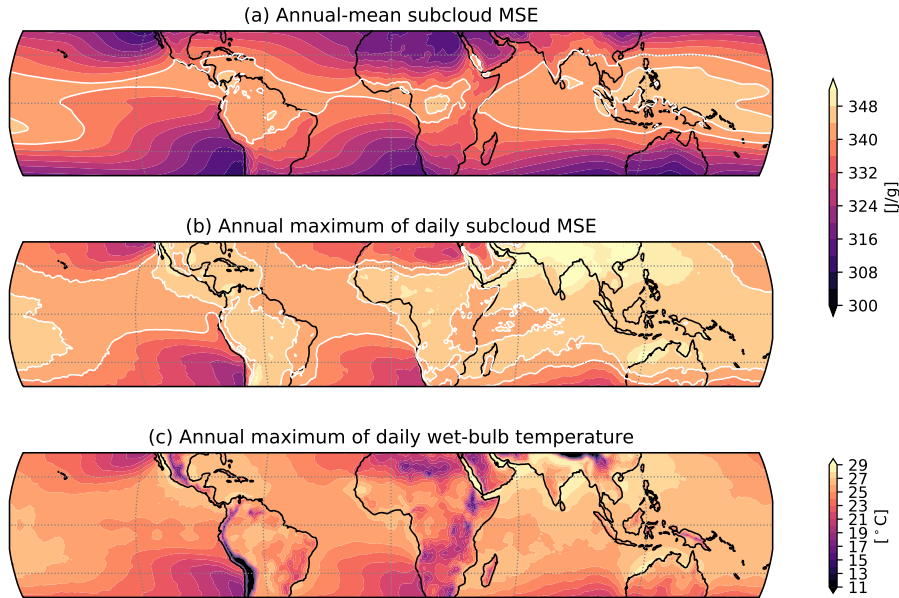

Figure S5. The annual-mean (a) and annual-maximum (b) daily-mean subcloud MSE and the annual-maximum daily 2-m wet-bulb temperature (c) from ERA-Interim averaged for 14 years within 2001-2014. White contours in (a) and (b) are to aid the comparison (The standard deviation is 8.8 J/g for panel (a) and 5.8 J/g for panel (b).)
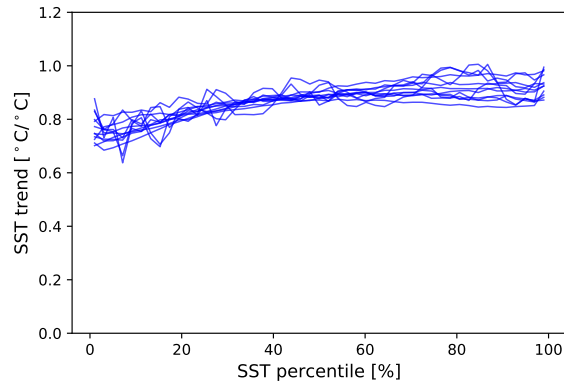
Figure S6. Trend of SST percentiles for each model normalized by tropical mean warming under RCP 8.5. Each line represents one CMIP5 model.
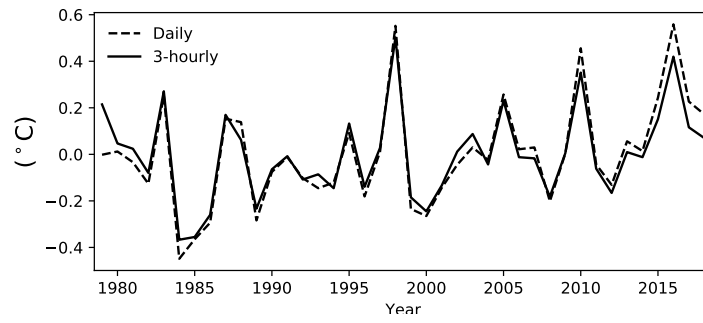

Figure S7. The tropical land-mean TW_{max} anomalies for TW_{max} defined as the annual-maximum daily-mean TW (dashed) and the annual-maximum 3-hourly TW (solid) for 1979-2018 from ERA-Interim.
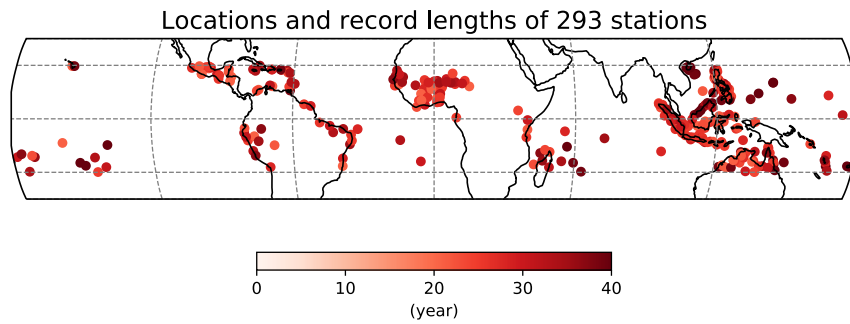

Locations and record lengths of 293 stations

Figure S8. Locations and record lengths (color) of 293 stations from HadISD that contain enough measurements required by this study.

Table S1. Table of CMIP5 models used in this study.

#	Model Name	Institute ID
1	ACCESS1-0	ACCESS
2	ACCESS1-3	ACCESS
3	CESM1-CAM5	NSF-DOE-NCAR
4	CNRM-CM5	CNRM-CERFACS
5	CSIRO-Mk3-6-0	CSIRO-QCCCE
6	CanESM2	CCCMA
7	GFDL-CM3	NOAA GFDL
8	GFDL-ESM2G	NOAA GFDL
9	GFDL-ESM2M	NOAA GFDL
10	HadGEM2-AO	NIMR/KMA
11	HadGEM2-CC	MOHC
12	HadGEM2-ES	MOHC
13	INMCM4	INM
14	IPSL-CM5A-LR	IPSL
15	IPSL-CM5A-MR	IPSL
16	IPSL-CM5B-LR	IPSL
17	MIROC5	MIROC
18	MIROC-ESM	MIROC
19	MIROC-ESM-CHEM	MIROC
20	MRI-CGCM3	MRI
21	MRI-ESM1	MRI
22	NorESM1-M	NCC